The baseline metabolism parameters of ^{18}F-FDG PET/CT as promising prognostic biomarkers in pediatric Langerhans cell histiocytosis

Xia Lu[1#], Ang Wei[2#], Guanyun Wang[1#], Junye Du[2], Lijuan Feng[1], Wenxin Ou[2], Tianyou Wang[2], Wei Wang[1], Jixia Li[3], Mingyu Zhang[1], Rui Zhang[2], Jigang Yang[1]

[1]Nuclear Medicine Department, Beijing Friendship Hospital, Capital Medical University, Beijing, China; [2]Hematology Center, Beijing Children's Hospital, Capital Medical University, National Center for Children's Health, Beijing, China; [3]Department of Laboratory Medicine, School of Medicine, Foshan University, Foshan, China

Contributions: (I) Conception and design: X Lu, A Wei, G Wang; (II) Administrative support: T Wang, R Zhang, J Yang; (III) Provision of study materials or patients: T Wang, R Zhang, J Yang; (IV) Collection and assembly of data: J Du, L Feng, W Ou; (V) Data analysis and interpretation: X Lu, G Wang, W Wang, J Li, M Zhang; (VI) Manuscript writing: All authors; (VII) Final approval of manuscript: All authors.

[#]These authors contributed equally to this work.

Correspondence to: Jigang Yang, MD. PhD. Nuclear Medicine Department, Beijing Friendship Hospital, Capital Medical University, 95 Yong'an Road, Xicheng District, Beijing 100050, China. Email: yangjigang@ccmu.edu.cn; Rui Zhang, MD, PhD. Hematology Center, Beijing Children's Hospital, Capital Medical University, National Center for Children's Health, 56 Nanlishi Road, Xicheng District, Beijing 100045, China. Email: ruizh1973@126.com.

Background: Langerhans cell histiocytosis (LCH) is a rare myeloid precursor cell inflammatory neoplasia, which agonizes, maims, and even kills patients. Although clinical outcomes have steadily improved over the past decades, the progression/relapse rate of LCH remains high. The purpose of this study was to evaluate the prognostic value of the pre-treatment metabolism parameters of baseline ^{18}F-fluorodeoxyglucose positron emission tomography/computed tomography (^{18}F-FDG PET/CT) in children with LCH.

Methods: This cross-sectional study retrospectively and consecutively included 37 children (24 males and 13 females; median age, 5.1 years; range, 2.4–7.8 years) with pre-treatment ^{18}F-FDG PET/CT from September 2020 to September 2022 in Nuclear Medicine Department, Beijing friendship hospital, Capital Medical University, Beijing, China. These patients were then all admitted to the hospital and diagnosed with LCH by biopsy, in Hematology Center, Beijing Children's Hospital, Capital Medical University, Beijing, China. Five metabolism parameters of ^{18}F-FDG PET/CT were analyzed, including maximum standardized uptake, tumor-to-normal liver standard uptake value ratio, tumor-to-normal bone marrow standard uptake value ratio, sum of metabolic tumor volume (sMTV), and sum of total lesion glycolysis (sTLG) of all lesions. Patients were followed up for at least 1 year or until disease progression/relapse. Univariate and multivariate analyses of progression-free survival was performed.

Results: During follow-up, 11 (29.7%) patients had disease progression/relapse. Univariate analysis revealed that the risk organ involvement, the treatment response at the 5th or 11th week, pre-treatment sMTV, and sTLG were significantly associated with progression-free survival (P=0.024, 0.018, 0.006, 0.006, and 0.042, respectively). Multivariate COX analysis revealed that non-response at the 11th week, pre-treatment sMTV >32.55 g/cm^{3}, and sTLG >98.86 g (P=0.002, 0.020, 0.026, respectively) were risk factors for progression-free survival.

Conclusions: The baseline metabolism parameters of ^{18}F-FDG PET/CT could be promising imaging biomarkers for predicting prognosis in children with LCH.

Introduction

Langerhans cell histiocytosis (LCH) is a rare myeloid precursor cell inflammatory neoplasia driven by mutations in the mitogen-activated protein kinase pathway (1). LCH usually occurs in children, and it is reported that the incidence rate of LCH is 4.46 cases per million children (<15 years old) every year, and the median age at diagnosis is 4 years old (2,3). From isolated eosinophilic granuloma to extensive diffuse disease with organ dysfunction, LCH shows a series of systemic involvement (4). The current classification of LCH is mainly based on the location of the lesion, the number of involved sites (single or multiple systems/local or multiple lesions) and whether risk organs (RO) are involved (hematopoietic system, liver or spleen) (5). The choice of treatment will be selected according to the classification of patients with LCH [single LCH (SS-LCH) or multiple systems LCH (MS-LCH)]; patients with SS-LCH confined to isolated skin lesions or a single bone lesion usually only need local treatment or observation, while patients with SS-LCH involved multiple lesions and MS-LCH need systemic treatment (6,7). The clinical patterns of LCH may vary remarkably, from single-system disease that may resolve spontaneously to refractory multisystem involvement with a 20% mortality (1). Although clinical outcomes have steadily improved over the past decades with standard-of-care chemotherapy and v-Raf murine sarcoma viral oncogene homolog B (*BRAF*) inhibitors for *BRAF* V600E-mutant disease, the disease relapse rates of multi-system LCH with risk organ involvement remain high, with recurrence rate of 30–50% (8).

Conventional imaging examinations, such as computed tomography (CT) or magnetic resonance imaging (MRI), and ultrasound can be used to assess the extent of involvement, guide biopsy and evaluate the treatment response (9-11). ^{18}F-fluorodeoxyglucose (^{18}F-FDG) positron emission tomography (PET)/CT plays an important role in evaluating LCH lesions, detecting new lesions, and monitoring treatment response (12,13). Compared with conventional imaging examination, ^{18}F-FDG PET/CT has a higher ability to detect lesions and can distinguish metabolically active lesions from inactive lesions (14). In the previous studies, ^{18}F-FDG PET/CT was shown to be highly sensitive for pretreatment and follow-up staging of pediatric LCH, with a very low false-positive rate (15,16). However, there is still no study on the prognostic value of ^{18}F-FDG PET metabolic parameters in children with LCH. In the current study, we aimed to investigate the prognostic role of ^{18}F-FDG PET/CT in children with LCH. We present this article in accordance with the STROBE reporting checklist (available at https://qims.amegroups.com/article/view/10.21037/qims-23-290/rc).

Methods

Patients

The study was conducted in accordance with the Declaration of Helsinki (as revised in 2013). The study was approved by the Ethics Committee of the Beijing Friendship Hospital, Capital Medical University and individual consent for this retrospective analysis was waived.

A total of 37 patients were retrospectively and consecutively included in this cross-sectional study, who underwent pre-treatment ^{18}F-FDG PET/CT in our institution with pathologically confirmed LCH between September 2020 and September 2022. The inclusion criteria consisted of (I) age less than 18 years old; (II) biopsy-proven LCH; (III) ^{18}F-FDG PET/CT scan performed within 30 days of the biopsy; (IV) followed up for at least 1 year or until disease progression/relapse. The exclusion criteria included the following: (I) patients who received LCH-related treatments such as chemotherapy, or targeted therapy prior to ^{18}F-FDG PET/CT examination; (II) patients with incomplete clinical data. The flow chart for patient selection is shown in *Figure 1*.

The baseline data of each patient were obtained by reviewing the medical records, which included the following aspects: (I) patients' demographics data, including age and gender; (II) clinical data, including clinical classification, involvement of organs at diagnosis, *BRAF*^{V600E} mutation status in the tissue, and targeted therapy protocol. The
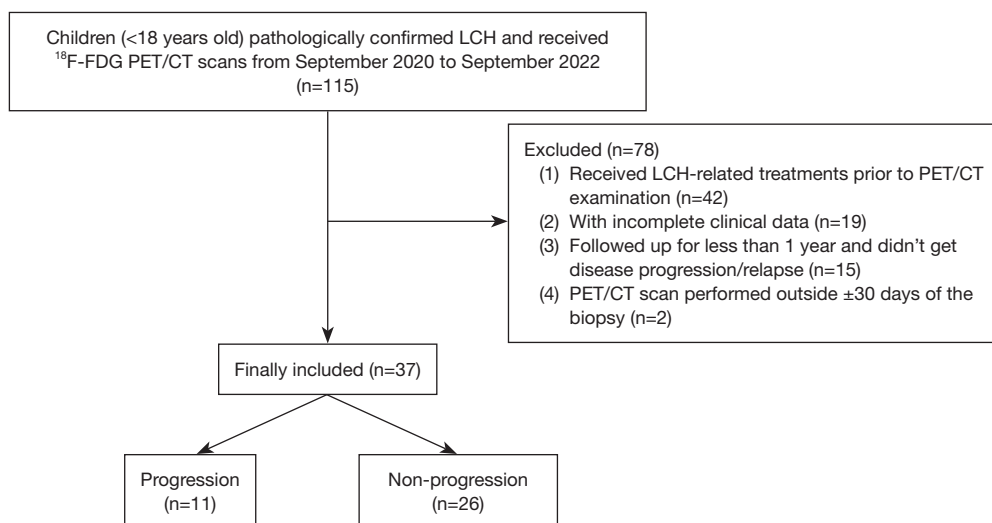
Figure 1 The flowchart of selection criteria. LCH, Langerhans cell histiocytosis; ¹⁸F-FDG, ¹⁸F-fluorodeoxyglucose; PET/CT, positron emission tomography/computed tomography.

tissue of LCH lesions was extracted at diagnosis for *BRAF^{V600E}* mutation analysis. The patients were classified as single-system (SS) LCH and multiple-system (MS) LCH based on the extent of involvement at diagnosis (5). RO involvement (RO+) was defined as liver, spleen, and/or hematologic system involvement. SS LCH was defined as only one organ or system involved and without RO involvement (RO–), while MS LCH was defined as two or more organs or systems involved either with or without RO involvement (RO+/RO–) (1).

PET/CT imaging acquisition

All patients in the cohort underwent whole body ¹⁸F-FDG PET/CT (Biograph mCT-64 PET/CT, Siemens Medical Solution) scans according to European Association of Nuclear Medicine guidelines for children tumor imaging at baseline (before starting chemotherapy) (17). Patients were instructed to fast for at least 6 hours, to make the blood glucose level under 11.1 mmol/L before the ¹⁸F-FDG injection. A mean dose of about 3.7 MBq/kg (0.10 mCi/kg) was administrated, considering the patients were children. If needed, infants were sedated using chloral hydrate 40 minutes after the ¹⁸F-FDG injection. About an hour after the injection, a low-dose CT scan (tube voltage 120 keV, thickness 3 mm) was performed for viewing anatomic structures and attenuation correction. A PET scan was performed immediately after CT acquisition in a three-

dimensional (3D) mode (2 min/bed position). PET images were reconstructed with the time-of-flight ordered subsets-expectation maximization algorithm.

Imaging analysis

Two experienced credentialed nuclear medicine physicians with more than 5-year experience in PET/CT diagnosis reviewed the PET/CT images on a dedicated workstation (syngo MultiModality Workplace, Siemens). They were blinded to the clinical information and reached a consensus for each lesion. Any disagreement would be discussed with another credentialed senior expert (experience >15 years) till reached an agreement. An involved lesion was determined with abnormal increased FDG uptake and/or with abnormal density on CT. A 3D volume of interest (VOI) of each lesion was drawn on the workstation with a threshold of 40% SUV_{max} (maximum standardized uptake), avoiding the nearby increased physiological uptake, such as brain physiological uptake. The SUV_{max}, metabolic tumor volume (MTV), and total lesion glycolysis (TLG) of each lesion were extracted. $SUVR_{liver}$ (tumor-to-normal liver standard uptake value ratio) was defined as the ratio of SUV_{max} of the lesion and SUV_{mean} (mean standardized uptake) of the liver, and the latter was determined by the mean FDG uptake of three 1-cm³-sized VOIs drawn in the normal liver. $SUVR_{BM}$ (tumor-to-normal bone marrow standard uptake value ratio) was defined as the ratio of SUV_{max} of the lesion and SUV_{max}

of the normal bone marrow, and the latter was determined by the maximum FDG uptake from the thoracic (T10-12) to lumbar (L1-4) vertebrae. The maximum SUV_{max}, maximum $SUVR_{liver}$, maximum $SUVR_{BM}$, sum of MTV (sMTV), and sum of TLG (sTLG) of all lesions in each patient were extracted for patient-based analysis.

Treatment and follow-up

Patients were treated with a systemic chemotherapy regimen BCH-LCH 2014 (http://www.chictr.org.cn, identifier: ChiCTR2000030457) (8), except for two patients (5.4%) who received $BRAF^{V600E}$ mutation targeted treatment (dabrafenib). Regular evaluation during treatment was undertaken at the 5th, 11th, 25th, and 52nd week after initial treatment. Then regular reviews at the 3rd, 6th month, 1st, 2nd, 3rd and 5th year were performed after drug withdrawal. The evaluation examination included hematological examination and imaging evaluation. Conventional imaging examinations, such as CT, MRI, and/or ultrasound, were usually performed during follow-up. Only a few patients underwent an ^{18}F-FDG PET/CT scan for evaluation. Treatment response was evaluated according to the International LCH Study Group Criteria (18,19). Nonactive disease (NAD) and active disease-better (AD-B) were defined as complete resolution, or continuous regression of disease, respectively. Active disease-stable (AD-S) was defined as unchanged disease. Active disease-intermediate (AD-I) was defined as unchanged disease or regression with some progressive or new lesions. Active disease-worse (AD-W) was defined as the progression of the existed lesions or the appearance of new lesions. Relapse was defined as the reappearance of active disease after either complete disease resolution or after a period of disease control that persisted for >3 months on maintenance therapy (20).

Patients were evaluated as non-response to treatment when they had AD-I or AD-W disease. Progression-free survival (PFS) was defined as the time between the initial diagnosis and the first disease progression (AD-I or AD-W) or relapse. Patients were followed up for at least 1 year or until disease progression/relapse. The last follow-up date was December 30, 2022. The median follow-up duration was 13.0 (95% CI: 12.4–13.6) months.

Statistical analysis

Data were analyzed with SPSS 24.0 software (IBM, Armonk, NY, USA); and R 4.0.2 software (Bell Laboratories, Holmdel, NJ, USA). Continuous variables with a normal or skewed distribution were reported as mean ± standard deviation and median (interquartile range), respectively. Categorical variables were reported as numbers (%). The difference of ^{18}F-FDG PET parameters between patients with and without disease progression/relapse was compared with student's t-test or Mann-Whitney U test. Spearman's correlation analysis was used to evaluate the relationships between variables. Univariate and multivariate analyses for PFS was performed using the Cox regression models. Receiver operating characteristic (ROC) curves and Youden index were calculated to determine the optimal cut-off value for multivariate analysis of PFS. Survival curves were obtained by the Kaplan-Meier method, and two-group comparisons were performed using the log-rank test. All tests were two-sided with a significance level of P<0.05.

Results

Patients' characteristic

Between September 2020 and September 2022, a total of 37 patients (24 males and 13 females; median age, 5.1 years; range, 2.4–7.8 years) were retrospectively included in this study. Nineteen (51.4%) patients were classified as SS-LCH, including 16 patients with a single-focal bone lesion and 3 patients with multiple bone lesions. And 18 (48.6%) were MS-LCH, of whom 5 with RO+. There were 17 (45.9%) patients with $BRAF^{V600E}$ mutation. During follow-up, 17 (45.9%) and 13 (35.1%) patients maintained non-response at the 5th and 11th week after the initial treatment, respectively. Eleven (29.7%) patients developed disease progression/relapse during follow-up. The clinical characteristics of the patients are summarized in *Table 1*.

Comparison of baseline ^{18}F-FDG PET/CT between patients with and without disease progression/relapse

The sTLG of the patients with disease progression/relapse was significantly higher than patients without disease progression/relapse after at least 1-year at follow-up [164.2 (2.23–230.16) *vs.* 23.7 (4.6–43.8), P=0.021]. There was no significant difference of SUV_{max} (7.8±5.1 *vs.* 5.6±3.4, P=0.133), $SUVR_{liver}$ (6.1±3.1 *vs.* 4.9±2.7, P=0.237), $SUVR_{BM}$ (4.1±2.0 *vs.* 3.2±1.7, P=0.164) and sMTV [44.9 (1.4–46.3) *vs.* 7.9 (2.5–11.7), P=0.181] between the two groups. The results are shown in *Table 2*.

Table 1 Patients' characteristics

Characteristics	Value (n=37)
Age (years)	5.1 (2.4–7.8)
Male sex	24 (64.9)
Clinical classification	
SS	19 (51.4)
Single-focal bone lesion	16 (43.2)
Multiple bone lesions	3 (8.1)
MS RO–	13 (35.1)
MS RO+	5 (13.5)
Involvement at diagnosis	
Central nervous system	1 (2.7)
Liver	4 (10.8)
Spleen	1 (2.7)
Hematologic system	0 (0.0)
Thyroid	6 (16.2)
Thymus	6 (16.2)
Lung	11 (29.7)
Pituitary	4 (10.8)
Skin	6 (16.2)
BRAF^{V600E} mutation	17 (45.9)
Targeted therapy at first diagnosis	2 (5.4)
Non-response at 5th week	17 (45.9)
Non-response at 11th week	13 (35.1)
Progression or relapse	11 (29.7)

The data are presented as number (proportion) of patients or median (interquartile range). SS, single-system; MS, multiple-system; RO, risk organ; *BRAF*, v-Raf murine sarcoma viral oncogene homolog B.

Prognostic value of baseline ^{18}F-FDG PET/CT on PFS

During follow-up, 11 (29.7%) patients showed disease progression/relapse. Univariate analysis revealed that the RO involvement [HR (95% CI): 4.835 (1.236–18.911), P=0.024], the worse treatment response at the 5th [HR (95% CI): 12.414 (1.548–99.556), P=0.018] or 11th [HR (95% CI): 9.173 (1.895–44.412), P=0.006] week, and higher sMTV [HR (95% CI): 1.030 (1.008–1.052), P=0.006] and sTLG [HR (95% CI): 1.005 (1.000–1.009), P=0.042] were significantly associated with shorter PFS (*Table 3*). The age,

gender, status of *BRAF*^{V600E} mutation, involvement of SS or MS, SUV$_{max}$, SUVR$_{liver}$, and SUVR$_{BM}$ were not significantly associated with PFS (*Table 3*). As a significant correlation was observed between treatment response at the 5th and 11th week (r=0.798, P<0.001), only the treatment response at the 11th week, with a lower P value, was analyzed in multivariate analysis. As a significant correlation was observed between sMTV and sTLG (r=0.964, P<0.001), sMTV and sTLG models were separately analyzed. ROC curves showed sMTV >32.55 g/cm^3 and sTLG >98.86 g were optimal cut-off values for predicting disease progression/relapse, with maximum Youden index of 0.52 and 0.48, respectively. Multivariate COX analysis revealed that non-response at the 11th week [16.162 (95% CI: 2.796–93.430), P=0.002], sMTV >32.55 g/cm^3 [7.960 (95% CI: 1.391–45.564), P=0.020] and non-response at 11th week [17.323 (95% CI: 2.934–102.290), P=0.002], sTLG >98.86 g [7.348 (95% CI: 1.274–42.377), P=0.026] were independent risk factors of PFS in sMTV and sTLG models, respectively (*Table 4*). Survival curves distinguished by these three biomarkers were shown in *Figure 2*. Two examples of patients with or without disease progression/relapse were shown in *Figures 3,4*. Two patients with both sMTV >32.55 g/cm^3 and sTLG >98.86 g, but kept disease regression with targeted therapy after over one-year follow-up, were shown in *Figure 5*.

Discussion

This is the first study on baseline ^{18}F-FDG PET/CT in predicting prognosis for pediatric LCH. Our study demonstrates the metabolism parameters of ^{18}F-FDG PET/CT as imaging biomarkers for predicting prognosis in children with LCH.

Overall outcomes have improved in LCH clinical trials over the past decades. However, disease progression and relapse remain the major causes of treatment failure and current main challenges for pediatric LCH. Therefore, it is essential to find prognostic biomarkers for PFS. Multi-system diseases account for about half of all children with LCH, 15% of which have risk organs involvement (21). The prognosis of MS-LCH is worse than SS-LCH, with a 5-year recurrence rate of 50% *vs.* less than 20% (1,19). Therefore, the accurate diagnosis of multi-system and risk organs involvement is of great value for the treatment guidance and prognosis of LCH patients. Studies have proved that ^{18}F-FDG PET has clinical value in diagnosing and classifying pediatric LCH (15,16). ^{18}F-FDG PET has also been shown to play a predictive role in the prognosis

Table 2 The difference of baseline ^{18}F-FDG PET parameters between patients with and without disease progression/relapse

Variable	Progression/relapse (n=11)	Non-progression/relapse (n=26)	P
SUV$_{max}$ (mean ± SD)	7.8±5.1	5.6±3.4	0.133
SUVR$_{liver}$ (mean ± SD)	6.1±3.1	4.9±2.7	0.237
SUVR$_{BM}$ (mean ± SD)	4.1±2.0	3.2±1.7	0.164
sMTV (g/cm^3), median (IQR)	44.9 (1.4–46.3)	7.9 (2.5–11.7)	0.181
sTLG (g), median (IQR)	164.2 (2.23–230.16)	23.7 (4.6–43.8)	0.021*

*, P<0.05. ^{18}F-FDG, ^{18}F-fluorodeoxyglucose; PET/CT, positron emission tomography/computed tomography; SD, standard deviation; IQR, interquartile range; SUV$_{max}$, max standard uptake value; SUVR$_{liver}$, tumor-to-normal liver standardized uptake value ratio; SUVR$_{BM}$, tumor-to-normal bone marrow standardized uptake value ratio; sMTV, sum of metabolic tumor volume; sTLG, sum of total lesion glycolysis.

Table 3 Univariate analysis of progression-free survival

Characteristics	Univariate analysis	
	HR (95% CI)	P
Age	1.129 (0.964–1.323)	0.133
Male vs. Female	1.621 (0.428–6.136)	0.477
BRAF^{V600E} mutation	0.416 (0.110–1.576)	0.197
SS vs. MS	98.712 (0.399–24,419.330)	0.102
RO– vs. RO+	4.835 (1.236–18.911)	0.024*
Non-response at 5th week	12.414 (1.548–99.556)	0.018*
Non-response at 11th week	9.173 (1.895–44.412)	0.006*
SUV$_{max}$	1.098 (0.939–1.282)	0.241
SUVR$_{liver}$	1.161 (0.905–1.489)	0.239
SUVR$_{BM}$	1.220 (0.830–1.793)	0.313
sMTV	1.030 (1.008–1.052)	0.006*
sTLG	1.005 (1.000–1.009)	0.042*

*, P<0.05. HR, hazard ratio; CI, confidence interval; BRAF, v-Raf murine sarcoma viral oncogene homolog B; SS, Single-system; MS, multiple-system; RO, risk organ; SUV$_{max}$, maximum standardized uptake values; SUVR$_{liver}$, tumor-to-normal liver standardized uptake value ratio; SUVR$_{BM}$, tumor-to-normal bone marrow standardized uptake value ratio; sMTV, sum of metabolic tumor volume; sTLG, sum of total lesion glycolysis.

of various childhood malignancies (14,22,23). SUV$_{max}$ is the most common semi-quantitative parameter of ^{18}F-FDG PET, which represents the highest glucose uptake in tumor or normal tissue. However, SUV$_{max}$ is measured from only one voxel, and thus could be affected by noise or artifact (24). Our study also did not show SUV$_{max}$, SUVR$_{liver}$ nor SUVR$_{BM}$ can predict the prognosis of LCH patients.

More studies have applied volumetric metabolic parameters to predict and evaluate the treatment response and prognosis of oncology patients (25,26). TLG is the mean SUV value of the region of interest multiplied by MTV, and MTV represents the size of tumor tissue that actively ingests ^{18}F-FDG (27). TLG and MTV reflect the tumor volume, tumor glucose activity, and the glucose metabolic state of tumor tissue (28), and the application of the sum of metabolic tumor (sTLG and sMTV) may reflect the tumor burden of patients more easily. Our results suggest that both baseline sTLG >98.86 g and sMTV >32.55 g/cm^3 can be used as independent risk factors to predict the PFS of pediatric LCH. This may be due to the fact that these patients had larger volumetric and metabolic tumor burdens, which lead to a worse treatment response. Therefore, these patients are more prone to recurrence or progression. In our study, two patients with BRAF^{V600E} mutation and MS-LCH showed persistent disease regression with target therapy (dabrafenib), even for those with high pretreatment tumor burden (sTLG >98.86 g and sMTV >32.55 g/cm^3, shown in *Figure 5*), which indicated that the targets therapy may be useful for these patients.

Meanwhile, the prognosis of LCH is also reported to depend on the age, the involvement of RO, and the response to initial systemic treatment (24,25). Some studies have shown that children under 2 years old with disseminated multisystem LCH and organ dysfunction have a poor prognosis (24). However, age was not associated with the PFS in our study. Cui *et al.* found that early treatment response (week 6) and the involvement of RO were independent risk factors for the PFS of children with LCH (29). In our study, we found the early treatment response at the 5th and 11th weeks was associated with PFS, and the treatment response at the 11th week was independently associated with PFS in both pre-treatment sMTV and sTLG models. In our study, we found that the involvement

Table 4 Multivariate analysis of progression-free survival

Characteristics	Multivariate analysis (sMTV model)		Multivariate analysis (sTLG model)	
	HR (95% CI)	P	HR (95% CI)	P
RO– vs. RO+	1.850 (0.371–9.226)	0.453	1.970 (0.391–9.925)	0.411
Non-response at 11th week	16.162 (2.796–93.430)	0.002*	17.323 (2.934–102.290)	0.002*
sMTV >32.55 g/cm^3	7.960 (1.391–45.564)	0.020*	–	–
sTLG >98.86 g	–	–	7.348 (1.274–42.377)	0.026*

*, P<0.05. HR, hazard ratio; CI, confidence interval; RO, risk organ; sMTV, sum of metabolic tumor volume; sTLG, sum of total lesion glycolysis.
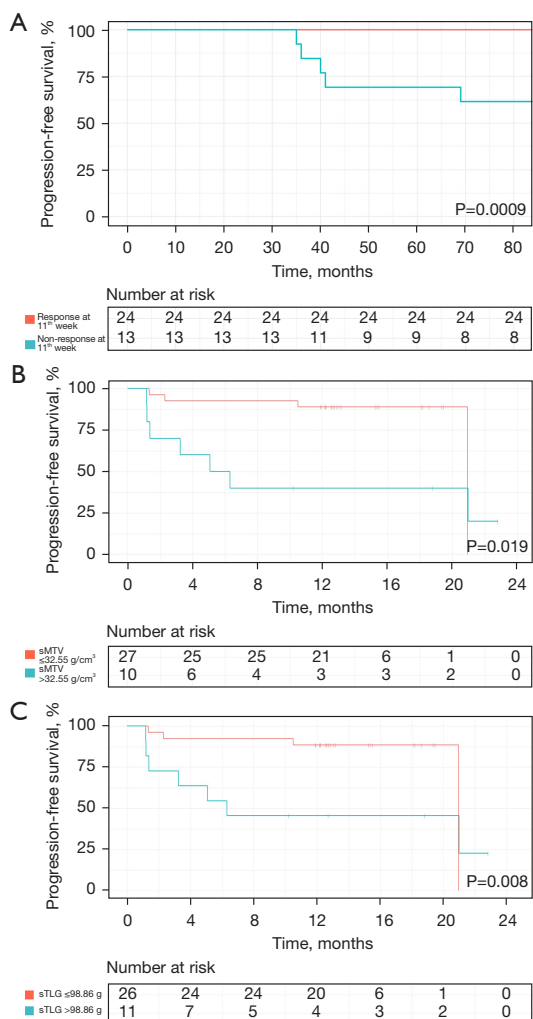

Figure 2 Kaplan-Meier curves for patients with Langerhans cell histiocytosis. (A) Patients with treatment response and non-response at 11th week (log-rank P=0.0009). (B) Patients with sMTV >32.55 and ≤32.55 g/cm^3 (log-rank P=0.019). (C) Patients with sTLG >98.86 and ≤98.86 g (log-rank P=0.008). sMTV, sum of metabolic tumor volume; sTLG, sum of total lesion glycolysis.

of RO was significant risk factor in univariate COX analysis, but not in multivariate analysis. Our result showed that the involvement of RO could affect the prognosis of patients, but could not predict prognosis independently. Moreover, it's reported that about 50% of children with LCH harbor *BRAF* mutations, which are associated with multi-system diseases (1). Patients with *BRAF* mutations have more treatment options, such as target therapy (dabrafenib and vemurafenib). BATF inhibitors, such as dabrafenib, have demonstrated clinical efficacy and manageable toxicity in relapsed/refractory *BRAF*^{V600}-mutant pediatric LCH (26). However, some studies showed there was no relationship between the *BRAF* mutations and prognosis (27,28). In our study, we also found that *BRAF* mutations did not relate to the prognosis of children with LCH. And even with *BRAF* mutations, only a few patients (2, 5.4%) in our study chose targeted therapy as the first line treatment.

Our present study had several limitations. First, this study is a retrospective study within a single center and a small sample (because LCH is a rare disease). Secondly, the median follow-up duration (13 months) was relatively short, which may provide a less accurate model of PFS. Third, due to the limitation of patient data collection, we did not analyze some possible prognostic factors (such as laboratory parameters and therapeutic regimen) (29,30). Fourth, many factors, such as blood glucose, fasting duration, uptake duration, and attenuation correction, may affect the measurement of metabolic parameters (25). Besides, the best cut-off value of ^{18}F-FDG PET metabolic parameters was selected by ROC, which may lead to the inconsistent selection of ^{18}F-FDG PET metabolic parameters under different clinical circumstances. Further studies should be done to assess more patients to find more accurate cut-off values. Moreover, as only 2 patients received targeted therapy in our study, our results may only be applicable to
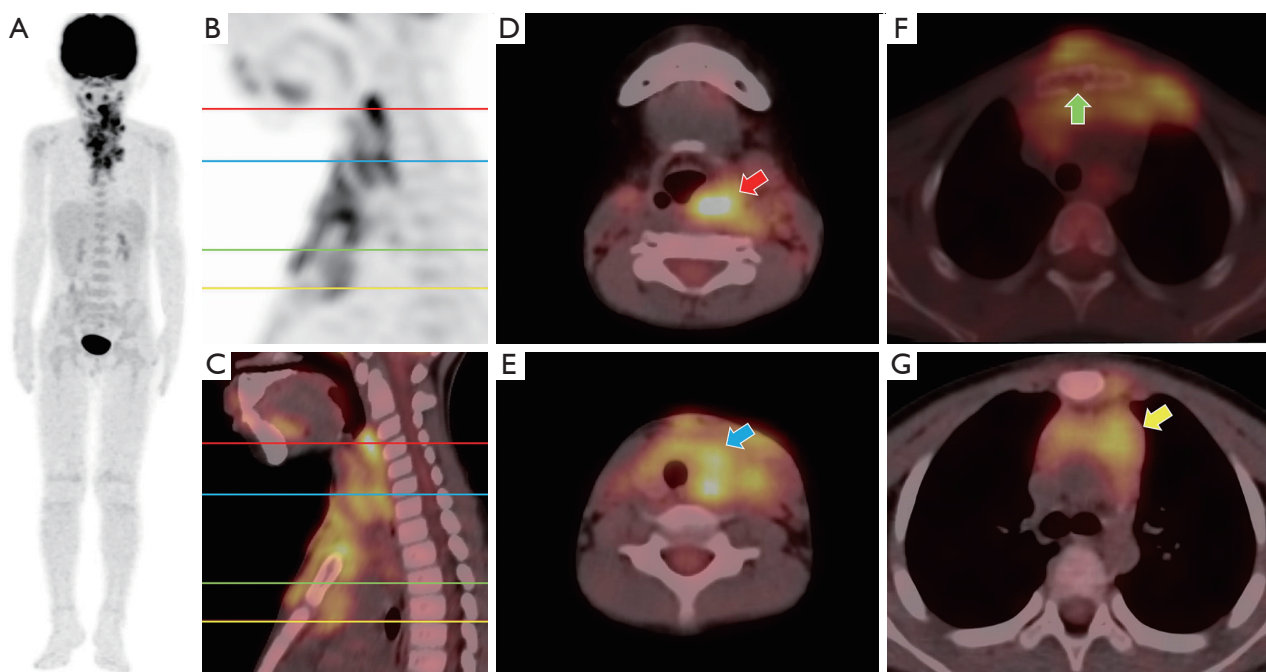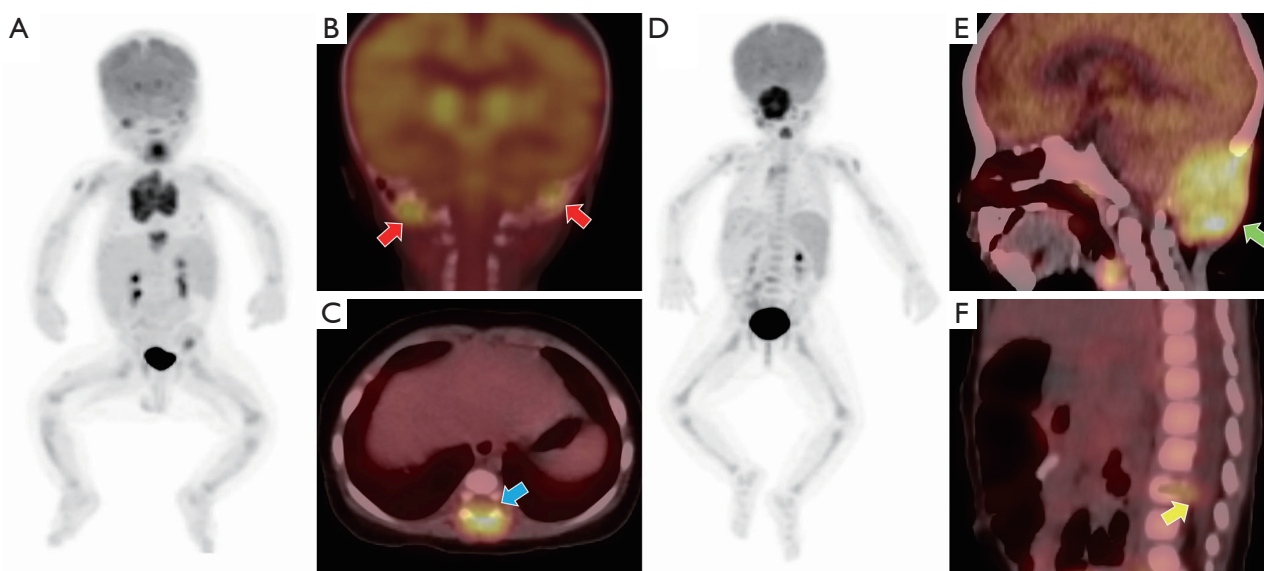
Figure 3 The baseline ^{18}F-FDG PET/CT images of a 5-year-old boy with pathologically diagnosed Langerhans cell histiocytosis. The maximum intensity projection image (A), sagittal PET (B), sagittal fused PET/CT (C), and axial fused PET/CT (D-G) images showed masses in the neck and anterior superior mediastinum, with elevated FDG uptake (SUV$_{max}$ 7.13, sMTV 44.92 g/cm^3, sTLG 176.90 g). The lines in B and C showed the involvement of the laryngopharynx (D, red arrow), thyroid (E, blue arrow), sternum (F, green arrow), and thymus (G, yellow arrow). *BRAF^{V600E}* gene mutation in the tissue was negative. Then he received first-line LCH chemotherapy and got disease regression (active disease-better) at the 5th and 11th-week evaluation. However, he got progression (active disease-intermediate) at the 5th-month evaluation, for enlarged lymph nodes in the neck. ^{18}F-FDG, ^{18}F-fluorodeoxyglucose; PET/CT, positron emission tomography/computed tomography; SUV$_{max}$, maximum standardized uptake values; sMTV, sum of metabolic tumor volume; sTLG, sum of total lesion glycolysis; *BRAF*, v-Raf murine sarcoma viral oncogene homolog B; LCH, Langerhans cell histiocytosis.
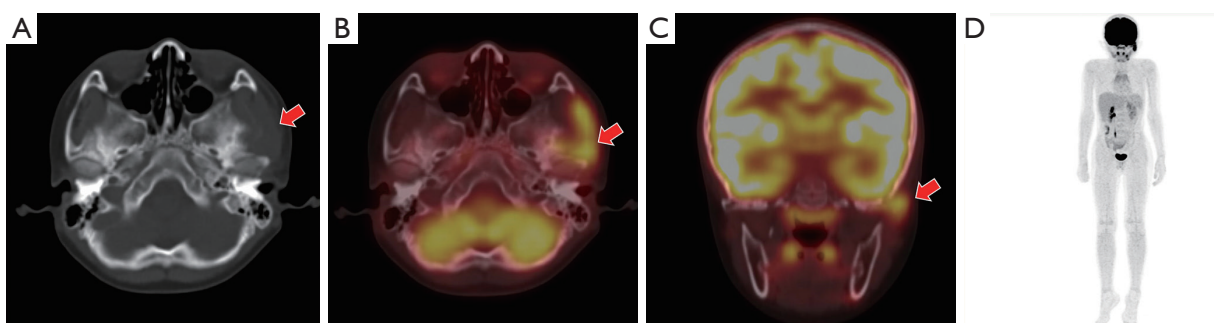
Figure 4 The baseline ^{18}F-FDG PET/CT images of a 7-year-old boy with pathologically diagnosed Langerhans cell histiocytosis. The axial CT (A), axial fused PET/CT (B), coronal fused PET/CT (C), and maximum intensity projection image (D) images showed bone destruction and mass of the zygomatic process of the temporal bone, with elevated FDG uptake (A-C, red arrow, SUV$_{max}$ 11.47, sMTV 10.29 g/cm^3, sTLG 65.37 g). *BRAF^{V600E}* gene mutation in the tissue was negative. He reached continuous regression of disease (active disease-better) during one-year first-line chemotherapy and six-month observation without therapy. ^{18}F-FDG, ^{18}F-fluorodeoxyglucose; PET/CT, positron emission tomography/computed tomography; SUV$_{max}$, maximum standardized uptake values; sMTV, sum of metabolic tumor volume; sTLG, sum of total lesion glycolysis; *BRAF*, v-Raf murine sarcoma viral oncogene homolog B.

Figure 5 The baseline ^{18}F-FDG PET/CT images of two patients with positive *BRAF^{V600E}* gene mutation in the tissue and received target therapy (dabrafenib) as first-line treatment. (A-C) Patient 1 is a 4-year-old boy. The maximum intensity projection image (A), coronary fused PET/CT (B), and axial fused PET/CT (C) showed multiple bone destruction in the skull (B, red arrow) and vertebrae (C, blue arrow), and masses in the thymus, skin and lungs, with elevated FDG uptake (SUV$_{max}$ 11.54, sMTV 56.31 g/cm^3, sTLG 349.39 g). He reached complete resolution (nonactive disease) after 16-month dabrafenib, then maintain stable after 5-month target therapy. (D-F) Patient 2 is a 10-year-old boy. The maximum intensity projection image (D), sagittal fused PET/CT (E), and sagittal fused PET/CT (F) showed a huge mass in the occipital bone (E, green arrow), which oppressing the cerebellum, and mass in the 4th lumbar vertebra (F, yellow arrow), which oppressing the vertebral canal, with elevated FDG uptake (SUV$_{max}$ 9.10, sMTV 43.63 g/cm^3, sTLG 246.95 g). He showed obvious diminution of the occipital mass after 1-month dabrafenib and reached continuous regression of disease (active disease-better) during 14-month target therapy. ^{18}F-FDG, ^{18}F-fluorodeoxyglucose; PET/CT, positron emission tomography/computed tomography; *BRAF*, v-Raf murine sarcoma viral oncogene homolog B; SUV$_{max}$, maximum standardized uptake values; sMTV, sum of metabolic tumor volume; sTLG, sum of total lesion glycolysis.

conventional therapies but not targeted therapies. In the future, we will continue to expand the sample size, conduct prospective research, and include more relevant prediction variables to ensure the accuracy and reliability of the study.

Conclusions

The non-response at 11th week, sMTV >32.55 g/cm^3 and sTLG >98.86 g could be risk factors of progression-free survival in pediatric LCH patients. The baseline metabolism parameters of ^{18}F-FDG PET/CT could be promising imaging biomarkers for predicting prognosis in children with LCH.

Acknowledgments

Footnote

Ethical Statement: The authors are accountable for all aspects of the work in ensuring that questions related

to the accuracy or integrity of any part of the work are appropriately investigated and resolved. The study was conducted in accordance with the Declaration of Helsinki (as revised in 2013). The study was approved by the Ethics Committee of the Beijing Friendship Hospital, Capital Medical University and individual consent for this retrospective analysis was waived.

Open Access Statement: This is an Open Access article distributed in accordance with the Creative Commons Attribution-NonCommercial-NoDerivs 4.0 International License (CC BY-NC-ND 4.0), which permits the non-commercial replication and distribution of the article with the strict proviso that no changes or edits are made and the original work is properly cited (including links to both the formal publication through the relevant DOI and the license). See: https://creativecommons.org/licenses/by-nc-nd/4.0/.

References

1. Krooks J, Minkov M, Weatherall AG. Langerhans cell histiocytosis in children: History, classification, pathobiology, clinical manifestations, and prognosis. J Am Acad Dermatol 2018;78:1035-44.
2. Liu H, Stiller CA, Crooks CJ, Rous B, Bythell M, Broggio J, Rankin J, Nanduri V, Lanyon P, Card TR, Ban L, Elliss-Brookes L, Broughan JM, Paley L, Wong K, Bacon A, Bishton M, West J. Incidence, prevalence and survival in patients with Langerhans cell histiocytosis: A national registry study from England, 2013-2019. Br J Haematol 2022;199:728-38.
3. Hu X, Buhtoiarov IN, Wang C, Sun Z, Zhu Q, Huang W, Yan W, Sun Y. Langerhans Cell Histiocytosis: A Population-based Study of Anatomical Distribution and Treatment Patterns. J Bone Oncol 2022;36:100454.
4. Allen CE, Merad M, McClain KL. Langerhans-Cell Histiocytosis. N Engl J Med 2018;379:856-68.
5. Rodriguez-Galindo C, Allen CE. Langerhans cell histiocytosis. Blood 2020;135:1319-31.
6. Gulati N, Allen CE. Langerhans cell histiocytosis: Version 2021. Hematol Oncol 2021;39 Suppl 1:15-23.
7. Rodriguez-Galindo C. Clinical features and treatment of Langerhans cell histiocytosis. Acta Paediatr 2021;110:2892-902.
8. Yao JF, Wang D, Ma HH, Lian HY, Zhang L, Wang TY, Li ZG, Jiang J, Cui L, Zhang R. Characteristics and Treatment Outcomes of Pediatric Langerhans Cell Histiocytosis with Thymic Involvement. J Pediatr

2022;244:194-202.e5.
9. Zhang X, Zhou J, Chai X, Chen G, Guo B, Ni L, Wu P. The application of x-ray, computed tomography, and magnetic resonance imaging on 22 pediatric Langerhans cell histiocytosis patients with long bone involvement: A retrospective analysis. Medicine (Baltimore) 2018;97:e0411.
10. Singh J, Rajakulasingam R, Saifuddin A. Langerhans cell histiocytosis of the shoulder girdle, pelvis and extremities: a review of radiographic and MRI features in 85 cases. Skeletal Radiol 2020;49:1925-37.
11. Della Valle V, Donadieu J, Sileo C, Barkaoui MA, Héritier S, Brisse H, et al. Chest computed tomography findings for a cohort of children with pulmonary Langerhans cell histiocytosis. Pediatr Blood Cancer 2020;67:e28496.
12. Luo ZH, Lu PX, Qi WL, Liao FX, Jin AF, Zen QY. Role of (18)F-FDG PET/CT in the diagnosis and management of patients with Langerhans cell histiocytosis. Quant Imaging Med Surg 2022;12:3351-63.
13. Liao F, Luo Z, Huang Z, Xu R, Qi W, Shao M, Lei P, Fan B. Application of (18)F-FDG PET/CT in Langerhans Cell Histiocytosis. Contrast Media Mol Imaging 2022;2022:8385332.
14. Ferrell J, Sharp S, Kumar A, Jordan M, Picarsic J, Nelson A. Discrepancies between F-18-FDG PET/CT findings and conventional imaging in Langerhans cell histiocytosis. Pediatr Blood Cancer 2021;68:e28891.
15. Jessop S, Crudgington D, London K, Kellie S, Howman-Giles R. FDG PET-CT in pediatric Langerhans cell histiocytosis. Pediatr Blood Cancer 2020;67:e28034.
16. Rameh V, Voss S, Bedoya MA, Beaulieu D, Zhang D, Degar BA, Tsai A. The added value of skeletal surveys in the initial evaluation of children diagnosed with Langerhans cell histiocytosis in the era of staging (18)F-FDG PET/CT: A retrospective study. Pediatr Blood Cancer 2023;70:e30057.
17. Stauss J, Franzius C, Pfluger T, Juergens KU, Biassoni L, Begent J, Kluge R, Amthauer H, Voelker T, Højgaard L, Barrington S, Hain S, Lynch T, Hahn K; . Guidelines for 18F-FDG PET and PET-CT imaging in paediatric oncology. Eur J Nucl Med Mol Imaging 2008;35:1581-8.
18. Haupt R, Minkov M, Astigarraga I, Schäfer E, Nanduri V, Jubran R, Egeler RM, Janka G, Micic D, Rodriguez-Galindo C, Van Gool S, Visser J, Weitzman S, Donadieu J; . Langerhans cell histiocytosis (LCH): guidelines for diagnosis, clinical work-up, and treatment for patients till the age of 18 years. Pediatr Blood Cancer 2013;60:175-84.
19. Gadner H, Minkov M, Grois N, Pötschger U, Thiem E,

Aricò M, Astigarraga I, Braier J, Donadieu J, Henter JI, Janka-Schaub G, McClain KL, Weitzman S, Windebank K, Ladisch S; . Therapy prolongation improves outcome in multisystem Langerhans cell histiocytosis. Blood 2013;121:5006-14.

20. Héritier S, Emile JF, Barkaoui MA, Thomas C, Fraitag S, Boudjemaa S, et al. *BRAF* Mutation Correlates With High-Risk Langerhans Cell Histiocytosis and Increased Resistance to First-Line Therapy. J Clin Oncol 2016;34:3023-30.

21. Rigaud C, Barkaoui MA, Thomas C, Bertrand Y, Lambilliotte A, Miron J, et al. Langerhans cell histiocytosis: therapeutic strategy and outcome in a 30-year nationwide cohort of 1478 patients under 18 years of age. Br J Haematol 2016;174:887-98.

22. Cheriyalinkal Parambil B, Shah S, Prasad M, Vora T, Laskar S, Khanna N, Qureshi S, Ramadwar M, Kembhavi S, Sankaran H, Rangarajan V, Thakur S, Chinnaswamy G. Can 18 F-FDG-Positron Emission Tomography be a Prognostic Tool in Children With Rhabdomyosarcoma Treated With Definitive Radiotherapy? J Pediatr Hematol Oncol 2023;45:e363-9.

23. Im HJ, Zhang Y, Wu H, Wu J, Daw NC, Navid F, Shulkin BL, Cho SY. Prognostic Value of Metabolic and Volumetric Parameters of FDG PET in Pediatric Osteosarcoma: A Hypothesis-generating Study. Radiology 2018;287:303-12.

24. Adams MC, Turkington TG, Wilson JM, Wong TZ. A systematic review of the factors affecting accuracy of SUV measurements. AJR Am J Roentgenol 2010;195:310-20.

25. Wen W, Piao Y, Xu D, Li X. Prognostic Value of MTV and TLG of (18)F-FDG PET in Patients with Stage I and II Non-Small-Cell Lung Cancer: a Meta-Analysis. Contrast Media Mol Imaging 2021;2021:7528971.

26. Burger IA, Casanova R, Steiger S, Husmann L, Stolzmann P, Huellner MW, Curioni A, Hillinger S, Schmidtlein CR, Soltermann A. 18F-FDG PET/CT of Non-Small Cell Lung Carcinoma Under Neoadjuvant Chemotherapy: Background-Based Adaptive-Volume Metrics Outperform TLG and MTV in Predicting Histopathologic Response. J Nucl Med 2016;57:849-54.

27. Wen W, Xu D, Piao Y, Li X. Prognostic value of maximum standard uptake value, metabolic tumour volume, and total lesion glycolysis of 18F-FDG PET/CT in patients with malignant pleural mesothelioma: a systematic review and meta-analysis. Cancer Cell Int 2022;22:60.

28. Cheng G, Huang H. Prognostic Value of (18) F-Fluorodeoxyglucose PET/Computed Tomography in Non-Small-Cell Lung Cancer. PET Clin 2018;13:59-72.

29. Cui L, Wang CJ, Lian HY, Zhang L, Ma HH, Wang D, Chen FF, Zhang Q, Yang Y, Wei A, Huang XT, Zhu T, Wang TY, Li ZG, Zhang R. Clinical outcomes and prognostic risk factors of Langerhans cell histiocytosis in children: Results from the BCH-LCH 2014 protocol study. Am J Hematol 2023;98:598-607.

30. Wang L, Yuan L, Du X, Zhou K, Yang Y, Qin Q, Yang L, Xiang Y, Qu X, Liu H, Qin X, Liu C. A Risk Model Composed of Complete Blood Count, *BRAF^{V600E}* and MAP2K1 Predicts Inferior Prognosis of Langerhans Cell Histiocytosis in Children. Front Oncol 2022;12:800786.